Arab J Sci Eng (2017) 42:4905–4916
DOI 10.1007/s13369-017-2741-6

RESEARCH ARTICLE - MECHANICAL ENGINEERING

# Optimization of Operational Parameters in Friction Stir Welding of AA7075-T6 Aluminum Alloy Using Response Surface Method

**A. Farzadi**[1] · **M. Bahmani**[2] · **D. F. Haghshenas**[1]

Received: 20 August 2016 / Accepted: 13 July 2017 / Published online: 20 July 2017


**Abstract** Response surface methodology was employed to optimize effective factors during friction stir welding of AA7075 aluminum alloy. The effect of operational parameters on the ultimate tensile strength of welded joints was studied. Five levels of the tool rotation speed, the welding speed, the shoulder diameter, and the pin diameter in the range of 350–650 rpm, 35–95 mm/min, and 12–18 and 4–6 mm were investigated using a central composite design. In order to have rotatable and orthogonal design, 36 experiments consisting of 12 center points were conducted. Moreover, the distance of each axial point from the center point was 2. All welded joints were defect free. The statistical model showed that the welding speed and the rotation speed compared to the shoulder diameter and the pin diameter have greater impact on the response. It was found that the joint efficiency of 85% was achievable under the intermediate rotational speeds and the high welding speeds using a tool with the moderate shoulder diameters and the large pin diameters. The joint produced using the rotation speed of 513 rpm and the welding speed of 95 mm/min, the shoulder diameter of 16.1 mm and pin diameter of 5 mm yielded the highest joint strength. This joint had a joint efficiency of about 94%.

**Keywords** Ultimate tensile strength (UTS) · Design of experiment (DOE) · Modeling · Second-order polynomial relationship · Interactions · Peak process temperature · Cooling rate

✉ A. Farzadi
farzadi@aut.ac.ir

[1] Department of Mining and Metallurgical Engineering, Amirkabir University of Technology, Hafez Ave., PO Box 15875-4413, Tehran 15916-34311, Iran

[2] Material Science and Engineering Department, Engineering Faculty, Shahid Chamran University, Ahvaz, Iran

## 1 Introduction

AA7075 aluminum alloy (Al–Zn–Mg–Cu) is one of the highest strength aluminum alloys in industrial use today. High strength, light weight, and natural aging characteristics make it attractive for aircraft structural applications and aerospace constructions. The high strength of AA7075 stems from $MgZn_2$ and $Al_2CuMg$ precipitates; moreover, the Cr-bearing phase ($Al_7Cr$) present in the structure provides the opportunity for controlling the grain structure. On the other hand, AA7075 aluminum alloy has relatively poor fusion weldability because it is susceptible to hot cracking in the fusion zone and the partially melted zone, and loss of strength due to overaging in the heat-affected zone (HAZ) during fusion welding processes [1].

Generally, in friction stir welding (FSW), as a solid-state joining process, a non-consumable rotating and traversing tool is employed to stir the material alongside the joint line. The contact between the tool and the workpiece material provides the heat required for reducing the material flow stress. The tool also produces the force required for plastic deformation. FSW can improve the weld-ability of high-strength precipitation-hardening 7xxx aluminum alloys [2,3]. The pertinent factors in the welding process significantly affect the joint properties through heat generation and material flow. Therefore, correct identification of the effect of the welding parameters such as rotation speed, welding speed, shoulder diameter, and pin diameter plays the crucial role in the mechanical properties and the consequent welding quality.

Various statistical and mathematical methods including regression, Taguchi, response surface methodology (RSM), and artificial neural network have been used by researchers to model the process parameters in friction stir welding [4–15]. However, RSM with central composite design has proved superior to predict responses, investigate influence of

parameters and identify an optimized point. Among numerous studies on FSW of aluminum alloys, only in limited works the design of experiment (DOE) strategies, particularly response surface methodology, have been applied for developing the models between the process variables and the mechanical properties, and optimization purposes. For instance, Rajakumar et al. [9] developed an empirical relationship to predict the tensile strength of friction-stir-welded AA7075–T6 aluminum alloy joints by RSM. Elangovan et al. [10,11] developed a mathematical model to predict the tensile strength of the friction-stir-welded AA6061 and AA2219 aluminum alloy by incorporating process parameters. Padmanaban and Balasubramanian [12] developed an empirical relationship to predict the tensile strength of friction stir-welded AZ31B magnesium alloy. Moreover, Safeen et al. [13] developed mathematical models for predicting mechanical properties of the friction-stir-welded AA6061-T6 joints using response surface methodology and found optimum conditions and examined influence of process parameters. The rotational speed was identified as more significant parameter than welding speed for ultimate tensile strength (UTS). Ghaffarpour et al. [14] optimized the FSW parameters in order to attain the highest tensile strength of tailored welded blank sheets made from aluminum alloys of 5083-H12 and 6061-T6. They showed that the rotational speed and the diameter tool had the most and the least effect on tensile strength, respectively. Ramachandran et al. [15] developed a central composite-response surface method model to predict the ultimate tensile strength of friction-stir-welded dissimilar aluminum alloy AA5052 H32 and HSLA steel IRS M-42-97. They reported that the UTS of the joint was very sensitive to the primary FSW parameters such as tool rotational speed, welding speed, axial force and tool tilt angle, and the ranges of FSW parameters that could produce substantial joint strength were very narrow. In most of these studies [4–12], the range of process parameters was wide, and hence some samples had a defect. However, the response of these samples were used to develop the models. Also, the effects of the process parameters on the joint strength are discussed without considering the interactions between parameters.

In the work presented in this paper, the influence of operational parameters on the joint strength of friction-stir-welded AA7075 aluminum alloy and the interaction between them were studied using response surface methodology (RSM). Rotation speed and welding speed as process factors and shoulder diameter and pin diameter as tool factors were considered in the model; besides, the optimal conditions were specified. It should be noted that the range of process parameters was specified by some preliminary welding experiments and FSW window was developed for AA7075-T6. In other words, all welded samples used in the model were sound and without defect.

## 2 Materials and Methods

### 2.1 Design of Experiments

Central composite design (CCD) was used as the experimental design in this study. Four factors, namely rotation speed, welding speed, shoulder diameter, and pin diameter, were investigated in five levels. Thirty-six experimental runs consisting of 16 ($2^4 = 16$) factorial points, eight axial points and twelve center points were generated according to the principle of response surface methodology (RSM) using MINITAB Release16. The distance of each axial point from the center, the value of $\alpha$, is 2. This value ($\alpha$) along with the number of center points were chosen to have a rotatable and orthogonal design. The experiments and levels employed for different parameters, based on the CCD, are given in Table 1.

It should be noted that numerous experiments had been performed to determine the process window before carrying out main runs. According to these preliminary welding experiments, the range of each factor were chosen to produce a sound and defect-free weld in all samples. In order to insure that the fabricated samples were defect free, all welded joints were cross-sectioned. Then, the cross sections were evaluated by visual inspection and under a light microscope. The macrostructure of the cross section of several samples is shown in Fig. 1. As it is apparent in the macrographs, the samples are free of any defect such as tunnel, excessive flash, lack of penetration, oxide entrapment nugget collapse, and material loss at anvil.

Assuming that a quadratic polynomial regression model can predict the response variable, $\sigma_{\text{uts}}$, a second-order polynomial equation is utilized to model the process. The second-order polynomial model in terms of the four independent factors is expressed by Eq. (1).

$$\sigma_{\text{uts}} = b_0 + \sum_{i=1}^{4} b_i x_i + \sum_{i=1}^{4} b_{ii} x_i^2 + \sum_{i=1}^{4} \sum_{j=2, i<j}^{4} b_{ij} x_i x_j \quad (1)$$

In Eq. (1), $\sigma_{\text{uts}}$ is the UTS of friction stir welded joints, $b_0$ is the intercept, $b_i$, $b_{ii}$ and $b_{ij}$ ($i$ and $j = 1, 2, 3$ and 4) are the coefficients of linear, quadratic and interaction terms, respectively.

Analysis of variance (ANOVA) was applied to evaluate whether the full quadratic model is statistically significant at 95% confidence level. In addition, accuracy and precision of the model were investigated using $P$ value and correlation coefficient. Based on these techniques, if the calculated value of the $P$ value for the developed model and their constants was less than the standard $P$ value (=0.05), the relation would be significant within the confidence limit. Finally, the model

was used to predict the optimum level of the factors resulting in maximum or fairly high UTS of the joint.

### 2.2 Experimental Procedure

AA7075-T6 aluminum alloy sheets with the thicknesses of 5 mm were used in this investigation. The composition of the as-received sheet was (by wt%): 5.6 Zn, 2.1 Mg, 1.2 Cu, 0.58 Si, 0.35 Fe, 0.12 Mn, 0.01 Ti, 0.19 Cr, and 0.01 Ni. The 250 × 100 mm pieces were extracted from the sheets and welding experiments were conducted under different conditions as listed in Table 1. The direction of welding was normal to the rolling direction. Friction stir welds were performed on the aluminum sheets using a 25 kW FSW machine

**Table 1** Results of ultimate tensile strength of friction-stir-welded joints based on design of experiment

| Factors | Uncoded welding parameters | | | | Coded welding parameters | | | | UTS |
|---|---|---|---|---|---|---|---|---|---|
| Symbol<br>Sample nos. | Rotation speed<br>*R*<br>(rpm) | Welding speed<br>*W*<br>(mm/min) | Shoulder diameter<br>*D*<br>(mm) | Pin diameter<br>*P*<br>(mm) | Rotation speed<br>A | Welding speed<br>B | Shoulder diameter<br>C | Pin diameter<br>D | $\sigma_{uts}$<br>(MPa) |
| 1 | 425 | 50 | 13.5 | 4.5 | −1 | −1 | −1 | −1 | 465 |
| 2 | 575 | 50 | 13.5 | 4.5 | 1 | −1 | −1 | −1 | 444 |
| 3 | 425 | 80 | 13.5 | 4.5 | −1 | 1 | −1 | −1 | 460 |
| 4 | 575 | 80 | 13.5 | 4.5 | 1 | 1 | −1 | −1 | 423 |
| 5 | 425 | 50 | 16.5 | 4.5 | −1 | −1 | 1 | −1 | 450 |
| 6 | 575 | 50 | 16.5 | 4.5 | 1 | −1 | 1 | −1 | 436 |
| 7 | 425 | 80 | 16.5 | 4.5 | −1 | 1 | 1 | −1 | 462 |
| 8 | 575 | 80 | 16.5 | 4.5 | 1 | 1 | 1 | −1 | 448 |
| 9 | 425 | 50 | 13.5 | 5.5 | −1 | −1 | −1 | 1 | 448 |
| 10 | 575 | 50 | 13.5 | 5.5 | 1 | −1 | −1 | 1 | 433 |
| 11 | 425 | 80 | 13.5 | 5.5 | −1 | 1 | −1 | 1 | 480 |
| 12 | 575 | 80 | 13.5 | 5.5 | 1 | 1 | −1 | 1 | 459.3 |
| 13 | 425 | 50 | 16.5 | 5.5 | −1 | −1 | 1 | 1 | 428 |
| 14 | 575 | 50 | 16.5 | 5.5 | 1 | −1 | 1 | 1 | 422 |
| 15 | 425 | 80 | 16.5 | 5.5 | −1 | 1 | 1 | 1 | 466 |
| 16 | 575 | 80 | 16.5 | 5.5 | 1 | 1 | 1 | 1 | 476 |
| 17 | 350 | 65 | 15 | 5 | −2 | 0 | 0 | 0 | 440.6 |
| 18 | 650 | 65 | 15 | 5 | 2 | 0 | 0 | 0 | 415 |
| 19 | 500 | 35 | 15 | 5 | 0 | −2 | 0 | 0 | 458 |
| 20 | 500 | 95 | 15 | 5 | 0 | 2 | 0 | 0 | 487 |
| 21 | 500 | 65 | 12 | 5 | 0 | 0 | −2 | 0 | 448 |
| 22 | 500 | 65 | 18 | 5 | 0 | 0 | 2 | 0 | 427 |
| 23 | 500 | 65 | 15 | 4 | 0 | 0 | 0 | −2 | 458 |
| 24 | 500 | 65 | 15 | 6 | 0 | 0 | 0 | 2 | 472 |
| 25 | 500 | 65 | 15 | 5 | 0 | 0 | 0 | 0 | 466 |
| 26 | 500 | 65 | 15 | 5 | 0 | 0 | 0 | 0 | 461.5 |
| 27 | 500 | 65 | 15 | 5 | 0 | 0 | 0 | 0 | 455 |
| 28 | 500 | 65 | 15 | 5 | 0 | 0 | 0 | 0 | 459.5 |
| 29 | 500 | 65 | 15 | 5 | 0 | 0 | 0 | 0 | 453 |
| 30 | 500 | 65 | 15 | 5 | 0 | 0 | 0 | 0 | 452 |
| 31 | 500 | 65 | 15 | 5 | 0 | 0 | 0 | 0 | 458 |
| 32 | 500 | 65 | 15 | 5 | 0 | 0 | 0 | 0 | 464 |
| 33 | 500 | 65 | 15 | 5 | 0 | 0 | 0 | 0 | 465 |
| 34 | 500 | 65 | 15 | 5 | 0 | 0 | 0 | 0 | 463 |
| 35 | 500 | 65 | 15 | 5 | 0 | 0 | 0 | 0 | 457 |
| 36 | 500 | 65 | 15 | 5 | 0 | 0 | 0 | 0 | 456 |

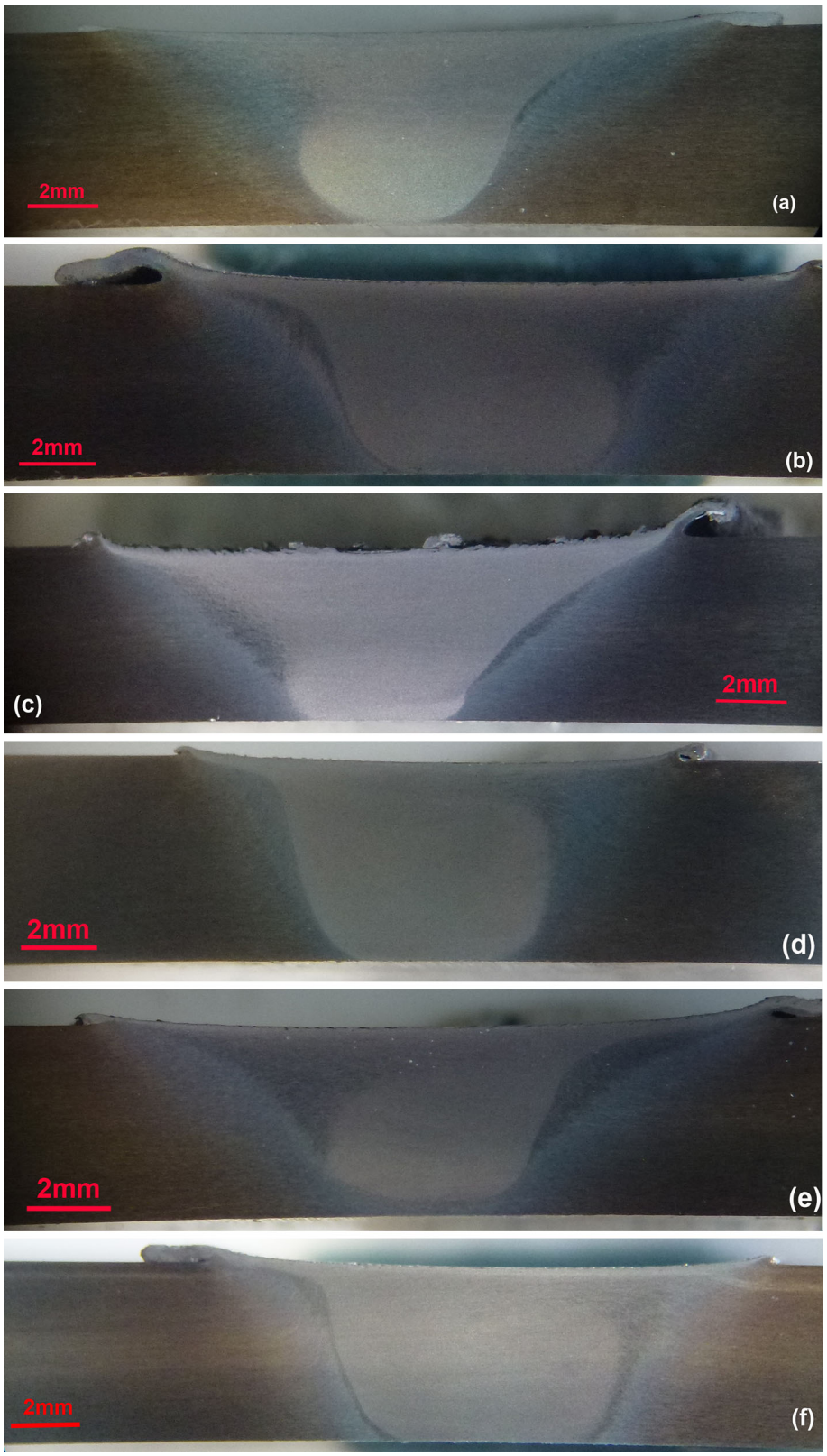


**Fig. 1** Optical microscope images showing cross-sectional macrostructure of the welded samples **a** 5, **b** 13, **c** 17, **d** 18, **e** 21 and **f** 22

(Model Stir Zone-IM5). Single-pass welding procedure was used to produce the square butt joints. The welding tools, consisted of a threaded cylindrical pin and a flat shoulder, made of hot die H13 steel and heat-treated to achieve the hardness of 52 Rockwell C. In this research, dwell time after plunge, backward tool tilt angle, and the thread pitch on the

pin, are kept constant at 10 s, 3° and 1 mm/thread, respectively. Six lateral mechanical clamps were used to secure two workpiece in position. During welding process, air with flow rate of 100 ml/min was blew to cool the weld zone behind the spindle.

In this study, chemical composition was determined using optical emission spectroscopy (OES). Small-size specimens (Type A) with the gage length of 50 mm were fabricated according to American Society for Testing of Materials (ASTM) standard E8 to evaluate the tensile properties. Three tensile specimens were extracted from each welded samples. The tensile test was carried out using a ZWICK 100 kN servo-controlled universal testing machine with a cross head speed of 5 mm/min at room temperature.

## 3 Results and Discussion

### 3.1 Model Fitting

The UTS of the 36 combinations of the factor levels limiting from 415 to 487 MPa is listed in Table 1. All tensile specimens failed outside the stir zone. In Fig. 2, the location of fracture in relation to the stir zone for several tensile specimens are presented. The fracture surfaces of the samples 17 and 18 are shown in Fig. 3. The fracture surface of these samples includes regions, which indicate the brittle fracture. These regions are surrounded by dimples, which are associated to the strengthening precipitates and indicate the ductile fracture. This type of the fracture is known as quasi-cleavage. This mode of the fracture has observed in the aluminum alloy AA7075 [16].

For determination of the regression coefficients of Eq. (1), the $P$ value of the regression coefficients (Table 2) were considered, i.e., a coefficient with $P$ value lower than 0.05 is significant and contributes to the final model. According to the results presented in Table 2, all linear terms as well as the second-order terms of the independent parameters, except for the pin diameter, $D^2$, are significant at 5% significance level. Moreover, the interaction between the rotation speed and the welding speed (AB), and the shoulder diameter and the pin diameter (CD) are not statistically significant.

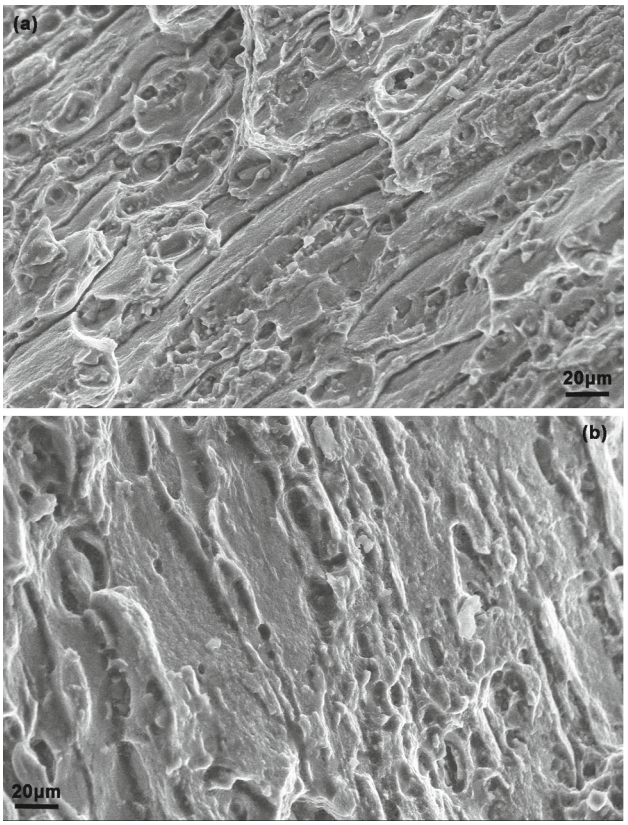


**Fig. 3** Scanning electron microscope micrographs of the fracture surfaces of the tensile specimens for the samples **a** 17 and **b** 18

The final coded statistical model for the prediction of UTS is expressed in Eq. (2).

$$\begin{aligned}\sigma_{\text{uts}}(\text{MPa}) = {} & 460.1 - 7.0A + 8.67B - 2.8C \\ & + 2.2D - 8.0A^2 + 3.2B^2 - 5.5C^2 \\ & + 4.4AC + 3.4AD + 5.2BC + 9.5BD \end{aligned} \quad (2)$$

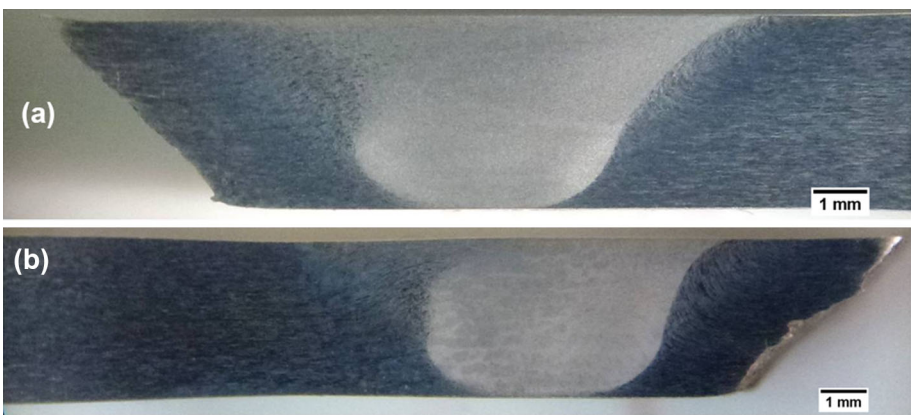


**Fig. 2** Macrographs of transverse tensile specimens showing the position of fracture and the SZ for the samples **a** 19 and **b** 20

**Table 2** Coefficients and their *P* values in coded condition

| Term | Coefficient | Standard error | *P* value |
|---|---|---|---|
| Constant linear | 459.167 | 1.4472 | 0.000 |
| *A* | −7.042 | 1.0233 | 0.000 |
| *B* | 8.597 | 1.0233 | 0.000 |
| *C* | −2.764 | 1.0233 | 0.013 |
| *D* | 2.181 | 1.0233 | 0.045 |
| Quadratic | | | |
| $A^2$ | 7.948 | 0.8862 | 0.000 |
| $B^2$ | 3.219 | 0.8862 | 0.002 |
| $C^2$ | 5.531 | 0.8862 | 0.000 |
| $D^2$ | 1.314 | 0.8862 | 0.144 |
| Interaction | | | |
| *AB* | −0.354 | 1.2533 | 0.780 |
| *AC* | 4.354 | 1.2533 | 0.002 |
| *AD* | 3.396 | 1.2533 | 0.013 |
| *BC* | 5.229 | 1.2533 | 0.000 |
| *BD* | 9.521 | 1.2533 | 0.000 |
| *CD* | 2.021 | 1.2533 | 0.122 |

In Table 3, ANOVA results for the second-order model, Equation (2), are listed. The ANOVA indicates that the regression of the model is appropriate (*P* value <0.0001); that is, the model is statistically significant. The *P* value corresponding to the lack of fit of the model is 0.359 (>0.05) and thus it is insignificant. As given in Table 3, the value of $R^2$, which indicates model fitting (goodness of fit), is 94.52% and acceptable for the developed model. Also, the value of adjusted $R^2$, $R^2$(adj), which indicates effectiveness of the model, is 90.86% and is acceptable.

**Table 3** The results of ANOVA test

| | *df* | SS | MS | *F* value | *P* value |
|---|---|---|---|---|---|
| Total | 35 | 9621.94 | – | – | – |
| Regression | 14 | 9094.19 | 649.59 | 25.85 | 0.000 |
| Residual error | 21 | 527.75 | 25.13 | – | – |
| Lack of fit | 10 | 280.58 | 28.06 | 1.25 | 0.359 |
| Pure error | 11 | 247.17 | 22.47 | – | – |
| $R^2$ | 94.52 | – | – | – | – |

*df* Degree of freedom, *SS* sum of squares, *MS*, mean squares

In order to confirm the regression model, a joint was prepared under the conditions given in Table 4. The experimental UTS of this joint was compared with the predicted value as following:

$$\text{Error } \% = \frac{\text{Real value} - \text{Predicted value}}{\text{Predicted value}} \times 100 \tag{3}$$

The percentage of error is 0.82, which indicates good ability of the model to predict the response.

### 3.2 Effect of Parameters on UTS

The influence of each parameter on the UTS of the friction stir welded joints was independently analyzed. For this purpose, the relationship between the UTS and the given parameter is evaluated by adjusting the level of other parameters at zero level.

The peak processing temperature and the cooling rate are important considerations during FSW process. In precipitation hardening aluminum alloys such as AA7075, the strengthening precipitates present in the base metal prior to FSW are generally dissolved in the stir zone (SZ), while these precipitates coarsen in the HAZ. The extent of the coarsening of precipitates or overaging depends on the cooling rate [17]. It is generally desirable to maintain a peak and working temperature as high as possible during FSW [18].

#### *3.2.1 Rotation Speed*

The variations of the UTS of the joints versus the rotation speed are shown in Fig. 4. By increasing the rotation speed, the UTS increases first and then decreases. The similar trend has been observed for precipitation-hardening aluminum alloys in the literature [8–10]. In these studies, it has been reported that the amount of heat due to friction increases in the higher rotation speeds and this leads to an excessive release of stirred material to the upper surface; consequently, the defects such as tunnel are produced in the SZ and the location of fracture shifts from a position with a minimum hardness in the HAZ for sound welds to the SZ [10,19]. However, the fracture site of all tensile specimens appears in the HAZ in this investigation and hence a reason that has been provided for a decrease in the strength by increasing the rotation speed cannot be acceptable here.

**Table 4** Comparison of predicted and experimental tensile strength in a different conditions from DOE

| Welding condition | Rotation speed (rpm) | Welding speed (mm/min) | Shoulder diameter (mm) | Pin diameter (mm) | Experimental UTS (MPa) | Predicted UTS (MPa) |
|---|---|---|---|---|---|---|
| Uncoded value | 450 | 60 | 15 | 5 | 462.5 | 458.72 |
| Coded value | −0.67 | −0.33 | 0 | 0 | | |

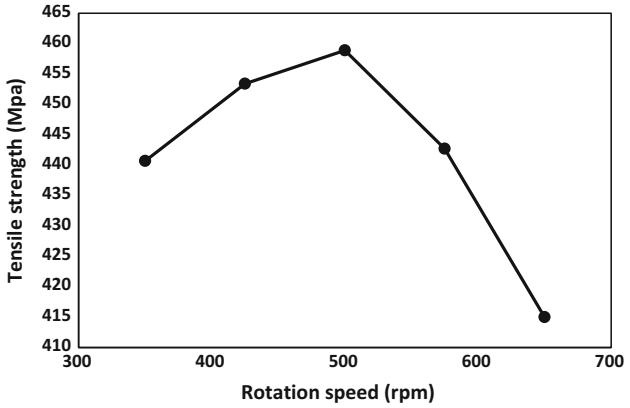


**Fig. 4** Variations in the UTS of joints with changes in the rotation speed

When the rotation speed increases from 350 to 500 rpm, the UTS reaches a maximum value of 458.9 MPa (Fig. 4). Above 500 rpm, the UTS of the joints decreases. The higher tool rotation speeds result in greater friction heating at the tool/workpiece interface. Up to 500 rpm, the peak process temperature and the size of SZ increases with increasing the rotation speed. As can be observed in Fig. 1c and f, the SZ of the sample 25 with the rotation speed of 500 rom is larger than that of the sample 17 with the rotation speed of 350 rpm. Furthermore, the cooling rate is seen to increase with increasing the working temperature [7,18]. Therefore, the UTS increases by increasing the lower rotation speeds due to the higher peak temperature and the cooling rate.

The peak process temperature saturates as the interface temperature and the heat generation are limited by rapid material softening at 500 rpm. The peak temperature increases to a point where workpiece material in the direct vicinity of the tool significantly loses flow strength. Thus strengthening, which would otherwise be anticipated to occur due to an increase in strain rate at the higher rotation speeds, cannot compensate for the effects of thermal softening. The shear stress between material at the tool/workpiece interface and the material far away it reduces. Due to the lower shear stress on the material far away the tool, this material cannot flow. Subsequently, material slip occurs at the tool/workpiece interface and the size of SZ decreases at the higher rotation speeds than 500 rpm. The heat generated by friction is transferred to the smaller volume of material, and the temperature in the SZ increases. As a consequence, the cooling rate decreases, the time required for phase transformation such as coarsening of precipitates, and the UTS decreases, since the thermal energy generated is not completely utilized for the development of the SZ. The similar behavior have been found in the literatures [13,14,20].

Note that Fig. 4 presents an intermediate rotation speed where the UTS is greatest. Therefore, the rotation speed of about 500 rpm can be considered as an optimum range for FSW aluminum alloy AA7075 because the peak process temperature and the cooling rate are maximum.

### 3.2.2 Welding Speed

The effect of the welding speed on the UTS of the joints is shown in Fig. 5. The UTS decreases first and then increases by the increase in the welding speed. As the welding speed increases, the power increases [21,22]. On the other hand, the heat input per unit length of weld can decrease when the welding speed increases. At the welding speeds slower than 50 mm/min, increasing the power is dominant, resulting in the slower cooling rate and decreasing the UTS. However, above 50 mm/min, the increase in the welding speed decreases the heat input per unit length of weld. This leads to the slower cooling rate and the shorter time for metallurgical transformation. In Fig. 6, microhardness distribution in the cross section of the samples 19 and 20 are shown. As can be seen in Table 1, the samples 19 and 20 were produced at the welding speeds of 35 and 95 mm/min, respectively. Minimum hardness for the both samples appears in the HAZ; however, the value of minimum hardness in the sample 19

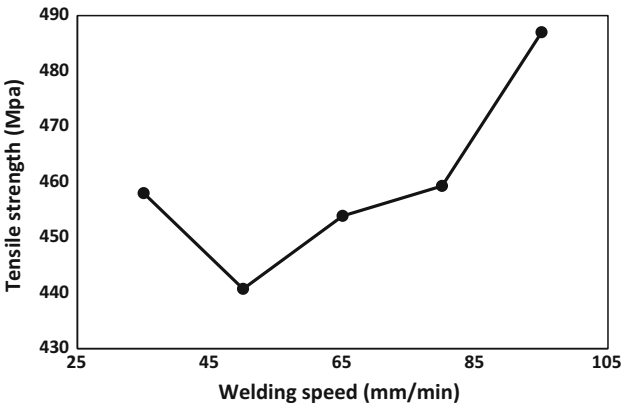


**Fig. 5** Effects of the welding speed on the UTS of joints

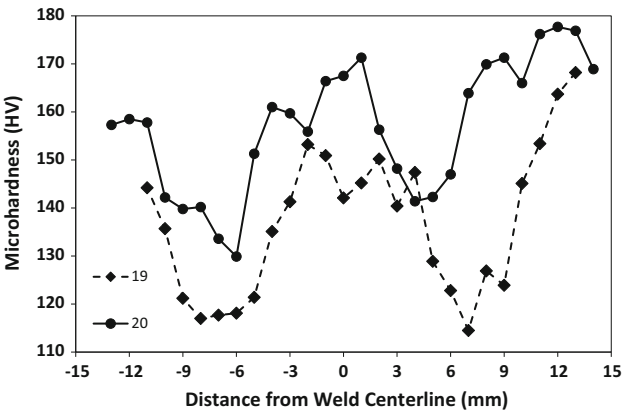


**Fig. 6** Vickers microhardness distribution in the weld cross section of the samples 19 and 20. Advancing side is on the right

is lower than that in the sample 20. Hardness variation in welded joints of precipitation-hardening aluminum alloys is significantly affected by welding thermal cycle, and the type and distribution of precipitates [23]. For the sample 19, the welding speed is low, and thus the heat input per unit length of weld is high and the cooling rate is slow. For this reason, coarsening of precipitates occurs, and the hardness and the UTS becomes lower.

The microstructure of several samples around the interface between the SZ and the thermo-mechanically affected zone (TMAZ) is shown in Fig. 7. The SZ consists of fine equiaxed grains. Adjacent to the stir zone, there is a zone known as TMAZ. In the TMAZ, the microstructure contains the deformed elongated grains, which changed their direction and drawn to the top side. Grain growth have been reported in the HAZ. However, most of changes in this zone are related to the metallurgical transformations such as reversion of precipitate, overaging, and solutionizing. For more details on the microstructure, the readers are referred to other text [24].

### *3.2.3 Shoulder Diameter*

The relationship between the UTS of the FSW joints and the shoulder diameter is shown in Fig. 8. The analogous variations are reported in the papers [8–10]. The UTS of the joints increases first and then decreases by enlargement of the shoulder diameter. In other word, both the small and the large shoulder diameters give rise to a loss of the UTS. The shoulder diameter and the rotation speed (Fig. 4) have similar effect on the UTS because both factors control the peak process temperature and the cooling rate. The larger shoulder diameter leads to the larger contact area between the tool and the workpiece. In the shoulder diameters below 15 mm, as the shoulder diameter enlarges, the peak process temperature promotes, the SZ increases in size, and the cooling rate becomes faster. As shown in Fig. 1d and e, the SZ of the sample 21 with the shoulder diameter of 12 mm is larger than that of the sample 22 with the shoulder diameter of 18 mm. The larger shoulder diameter than 15 mm can decrease the cooling rate and increase the time available for metallurgical transformations, i.e., the bigger precipitates form in the HAZ and also the width, where coarsening occurs, is enlarged. Microhardness profile in the cross section of the samples 21 and 22 is demonstrated in Fig. 9. The samples 21 and 22 are produced by the shoulder diameter of 12 and 18 mm, respectively. The size of a region where hardness is low is larger for the sample 22 and its minimum hardness is lower (Fig. 9). The results show that when the shoulder diameter increases, both the size of a region where the precipitates grow and the time for coarsening of precipitates increase, and hence both the hardness and the UTS increase.

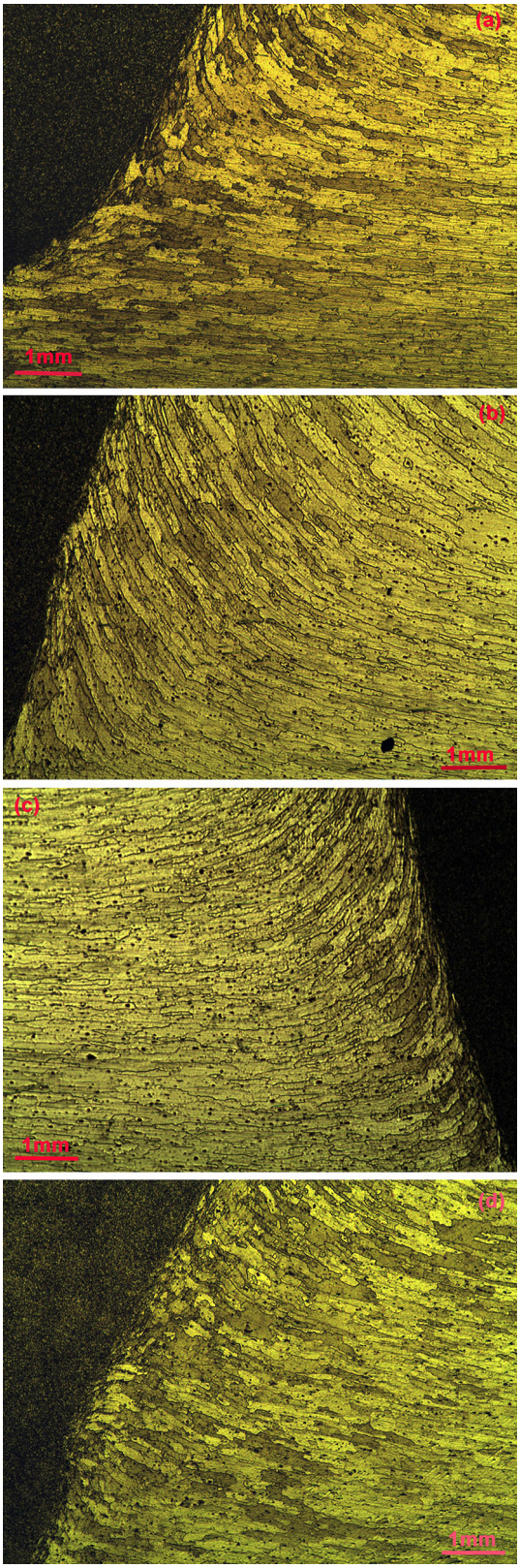


**Fig. 7** Optical micrographs of the microstructure for the samples **a** 18, **b** 20, **c** 21, **d** 22

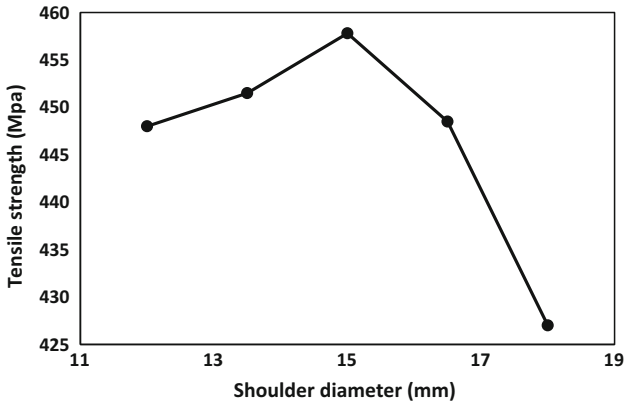


**Fig. 8** Relationship between the UTS of joints and the shoulder diameter

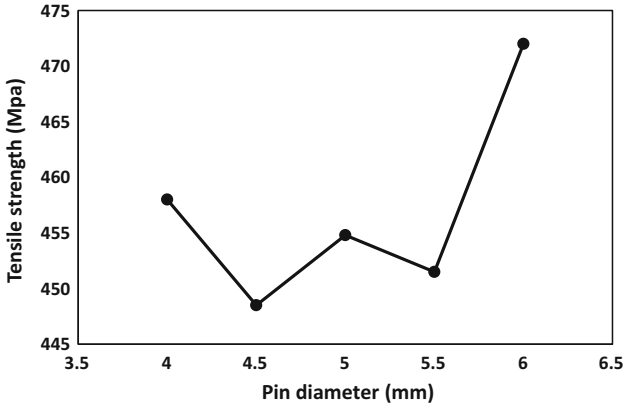


**Fig. 10** UTS of joints as a function of the pin diameter

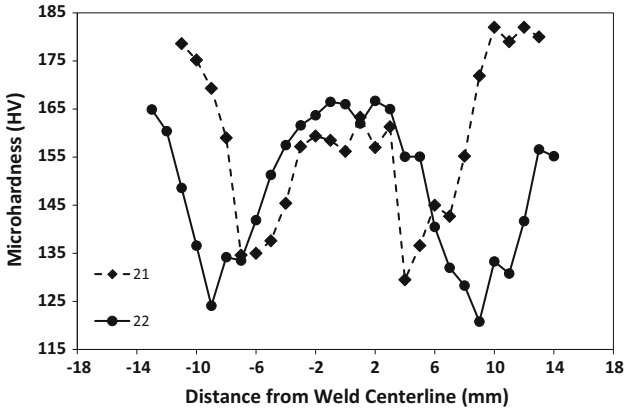


**Fig. 9** Vickers microhardness distribution in the weld cross section of the samples 21 and 22. Advancing side is on the right

### *3.2.4 Pin Diameter*

The changes of the UTS with the pin diameter are shown in Fig. 10. The UTS of the joints increases with the pin diameter. This is because of the fact that with enlargement of the pin diameter, the SZ become larger and the process heat input is transferred to the larger volume of material, resulting in reducing the cooling rate in the HAZ. As can be observed in Fig. 1a and b, the SZ of the sample 4.5 with the pin diameter of 4 mm is larger than that of the sample 13 with the pin diameter of 5.5 mm. The similar results were reported by Rajakumar [8,14]. By comparison with the other factors, the pin diameter has the smaller impact on the UTS. On average, increasing the pin diameter from 4.5 to 6 mm results in a 24 MPa increase in the UTS. However, increasing the rotation speed by the same factor (500–650 rpm) causes the UTS to increase by 44 MPa.

Although, by increasing the pin diameter, the contact area between the tool and the workpiece increases, the heat generated by the pin, $Q_p$, is considerably smaller than the heat generated by the shoulder, $Q_s$. In this investigation, the ratio of $Q_s$ to $Q_p$ is 7.7 (87–17%) [25].

## 3.3 Interactions of Parameters

In the cases where interaction between the factors is statistically significant, surface plots give more complete information regarding the effect of factors on the response.

### *3.3.1 Welding Speed and Shoulder Diameter*

The effects of the welding speed ($W$) and the shoulder diameter ($D$) on the UTS of the joints are exhibited Fig. 11 when the rotation speed and the pin diameter are 500 rpm and 5 mm, respectively. Joint efficiency, which is expressed as a percentage, is the ratio of the UTS of a joint to the UTS of the base metal. The area where the joints have a UTS above 484.5 MPa (joint efficiency of 85%) is observed in the high welding speed and the moderate to large shoulder diameter. As the welding speed increases, the heat input per unit length of weld and the width of the SZ decrease, the cooling rate raises, and thus there is less time for solid-state transformation. With increasing the shoulder diameter, due to the larger contact area between the tool and the workpiece, the peak process temperature increases and the cooling rate reduces. As mentioned before, the loss of the strength in AA7075 aluminum alloy joints is due to the coarsening of the $\eta'$ precipitates and the dissolution of the fine particles (GP zones) in the HAZ [17,26]. These processes depend on solid-state diffusion, which requires both the time and the adequate temperature. The time required for the solid-state diffusion decreases by increasing the welding speed and the heat input.

Contrary to the small area associated with joint efficiency above 0.85, the area where the UTS of the joints is higher than 456 MPa (joint efficiency is 80%) is large. At all welding speeds, joint efficiency of 80% is achievable provided that

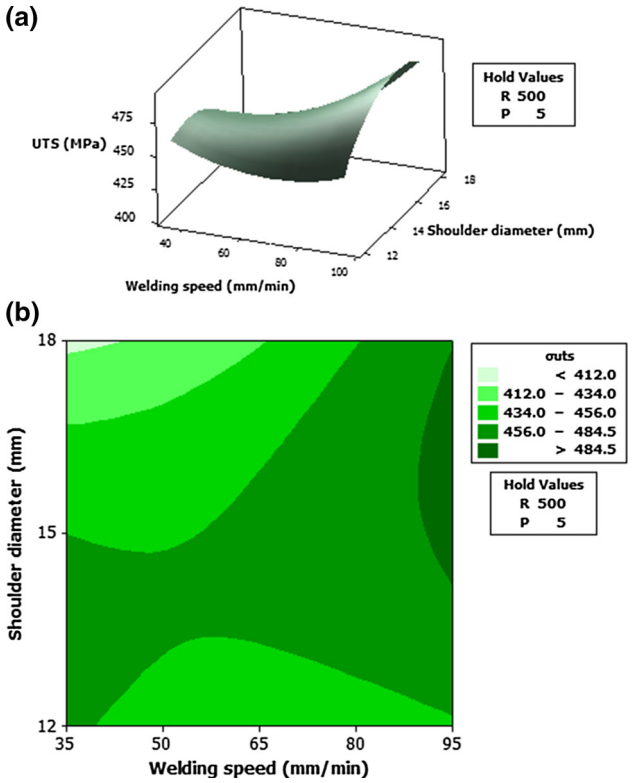


**Fig. 11** **a** Surface and **b** contour plot for the UTS of joints with respect to the welding speed and shoulder diameter (the rotation speed and pin diameter are at the zero level)

the shoulder diameter is correctly specified. At the higher welding speeds, the proper range of the shoulder diameter is wider. The narrowest range of the shoulder diameter is observed from 45 to 60 mm/min.

When the welding speed is minimum (35 mm/min) and the shoulder diameter is maximum (18 mm), the heat input significantly increases and the area with the strength below 412 MPa is observed (Fig. 11). The slow welding speed and the large shoulder diameter can increase the heat input, decrease the cooling rate, and increase the retention time required for metallurgical transformation. Therefore, in order to achieve high-strength welded joints (joint efficiency of 85%), the high welding speed (90–95 mm/min) and the moderate shoulder diameter (14.2–17.8 mm) must be chosen (Fig. 11).

In Eq. (2), the coefficients corresponding to the terms B and $B^2$ are higher than those of C and $C^2$ which indicates the welding speed is more effective factor than the shoulder diameter. The term BC indicates the interaction between the two variables of the welding speed and the shoulder diameter. According to Eq. (2), the term BC has the highest effectiveness and the joint strength improves when the welding speed and the shoulder diameter are set at coded level +2. If one of the parameters is set at +1 or +2 and the other is set at −1 or −2, the term BC becomes negative and the joint strength decreases. Thus, in the cases that one of the parameters is positive and the other is negative, the interaction of two parameter has insignificant influence on the joint strength. On the other hand, the combination of the high welding speed and the low shoulder diameter or the low welding speed and the high shoulder diameter leads to the relatively low joint strength.

### *3.3.2 Rotation Speed and Shoulder Diameter*

The variations of the UTS of the joints versus the rotation speed ($R$) and the shoulder diameter ($D$) are shown in Fig. 12 when the welding speed is 65 mm/min and the pin diameter is 5 mm. The rotation speed and the shoulder diameter significantly affect the heat generation process in FSW. In addition to the heat generation, the shoulder prevents existing soft materials from the weld zone and leads to returning the materials to the weld zone [18]. Also, the rotation speed influences material stirring and mixing in the SZ. As both the rotation speed and the shoulder diameter increase, the heat input increases, the cooling rate diminished, and the joint strength decreases to below 412 MPa. The area where have the maximum joint strength (>456 MPa or joint efficiency

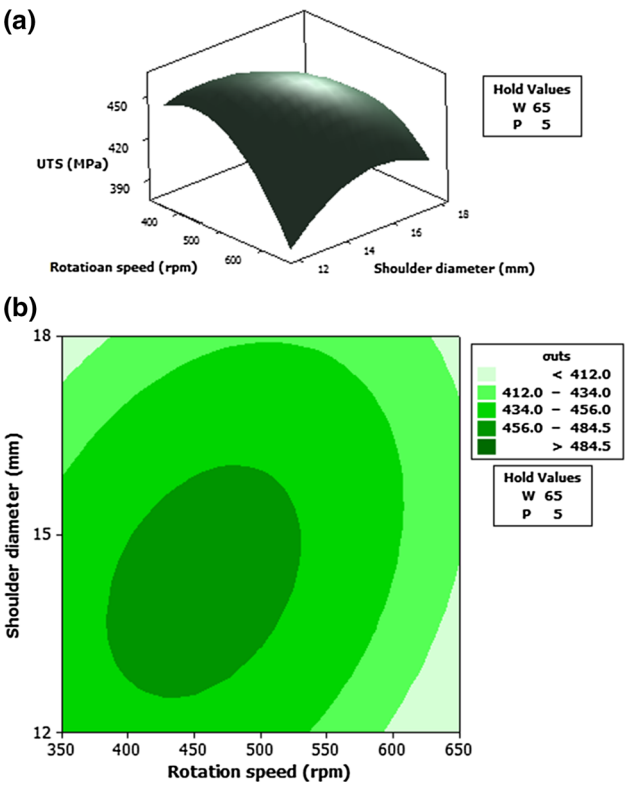


**Fig. 12** **a** Surface and **b** contour plot of the UTS of joints versus the rotation speed and shoulder diameter (the welding speed and pin diameter are at the zero level)

**Table 5** Optimum conditions for FSW of AA7075-T6 aluminum alloy

| Welding parameter | Rotation speed (rpm) | Welding speed (mm/min) | Shoulder diameter (mm) | Pin diameter (mm) |
|---|---|---|---|---|
| Coded value | 0.1818 | 2 | 0.7483 | 2 |
| Real value | 513.65 | 95 | 16.12 | 6 |

of 80%) is in the rotation speeds of 380–530 rpm and the shoulder diameters of 12.5–16 mm. It can be noted that the peak process temperature and the cooling rate are high in these ranges and hence a large SZ is produced while time required for the metallurgical transformation is not high.

In Eq. (2), the coefficients of A and $A^2$ are higher than those of C and $C^2$, which indicates the rotation speed has a more significant effect on the joint strength. At the positive coded levels of the rotation speed and the shoulder diameter, both of them have negative effect on the joint strength.

### 3.4 Optimization of Process Parameter

The optimization of a combination of the factor levels for achieving the maximum UTS of the friction stir-welded joints was carried out using the proposed second-order polynomial model (Eq. 2). The optimum conditions are given in Table 5. The predicted value of the UTS and the joint efficiency in the optimum conditions are 535.5 MPa and 94%, respectively.

Furthermore, the optimal range of the rotation speed, the welding speed, the shoulder diameter and the pin diameter to produce a friction stir-welded joint with the joint efficiency of 85% is 380–530 rpm, 90–95 mm/min, 14.2–17.8 and 5–6 mm, respectively.

## 4 Conclusions

Modeling of FSW process was successful and the second-order polynomial relationship between four factors including the rotation speed, the welding speed, the shoulder diameter and the pin diameter, and the UTS of friction stir-welded AA7075 aluminum alloy joints was developed using the CCD-RSM. The major results are as follows:

(1) According to the coded equation (Eq. 2), the most effective parameters on the UTS, response, are the welding speed, the rotation speed, the shoulder diameter and the pin diameter, respectively. The welding speed has the most significant influence on the UTS.
(2) The interaction between all factors except the rotation speed and the welding speed as well as the shoulder diameter and the pin diameter is statistically significant.
(3) Based on the contour plot of the interaction between the rotation speed and the shoulder diameter on UTS, the area where have the maximum joint strength (>456 MPa or joint efficiency of 80%) is in the rotation speeds of 380–530 rpm and the shoulder diameters of 12.5–16 mm. The peak process temperature and the cooling rate are high in these ranges and hence a large SZ is produced, while time required for the metallurgical transformation is not high.
(4) The joint efficiency of 94% (the UTS of 513 MPa) can be obtained under the optimum welding conditions of 514 rpm and 95 mm/min by using a tool consisting of a shoulder with diameter of 16.1 mm and a pin with diameter of 6 mm. Also, the joint efficiency of 85% is achievable under the operational parameters: the rotation speed of 380–530 rpm, the welding speed of 90–95 mm/min, the shoulder diameter of 14.2–17.8 mm and the pin diameter of 5–6 mm.

**Acknowledgements** The authors are pleased to acknowledge the experimental assistance of Mr. Pouladgar, Laboratory Manager of Iran National Steel Industrial Group. We are also grateful to Mr. Zaeri, Direct Manager of Azin Sanaat Farasoo (ASF) Co., for providing the FSW Machine.

## References

1. Hassan, K.A.A.; Prangnell, P.B.; Norman, A.F.; Price, D.A.; Williams, S.W.: Effect of welding parameters on nugget zone microstructure and properties in high strength aluminium alloy friction stir welds. Sci. Technol. Weld. Join. **8**, 257–268 (2003)
2. Goloborodko, A.; Ito, T.; Yun, X.; Motohashi, Y.; Itoh, G.: Friction stir welding of a commercial 7075-T6 aluminum alloy: grain refinement, thermal stability and tensile properties. Mater. Trans. **45**, 2503–2508 (2004)
3. Reynolds, A.P.; Tang, W.; Khandkar, Z.; Khan, J.A.; Lindner, K.: Relationships between weld parameters, hardness distribution and temperature history in alloy 7050 friction stir welds. Sci. Technol. Weld. Join. **10**, 190–199 (2005)
4. Rajakumar, S.; Muralidharan, C.; Balasubramanian, V.: Statistical analysis to predict grain size and hardness of the weld nugget of friction-stir-welded AA6061-T6 alumimium alloy joints. Int. J. Adv. Manuf. Technol. **57**, 151–165 (2011)
5. Rajakumar, S.; Balasubramanian, V.: Correlation between weld nugget grain size, weld nugget hardness and tensile strength of friction stir welded commercial grade aluminium alloy joints. Mater. Des. **34**, 242–251 (2011)
6. Lakshminarayanan, A.K.; Balasubramanian, V.: Comparison of RSM with ANN in predicting tensile strength offriction stir welded AA7039 aluminium alloy joints. Trans. Nonferr. Met. Soc. China **19**, 9–18 (2009)
7. Rajakumar, S.; Balasubramanian, V.: Establishing relationships between mechanical properties of aluminium alloys and optimised friction stir welding process parameters. Mater. Des. **40**, 17–35 (2012)
8. Lakshminarayanan, A.K.; Balasubramanian, V.: Process parameters optimization for friction stir welding of RDE-40 aluminium alloy using Taguchi technique. Trans. Nonferr. Met. Soc. China **18**, 548–554 (2008)

9. Rajakumar, S.; Muralidharan, C.; Balasubramanian, A.K.: Influence of friction stir welding process and tool parameters on strength properties of AA7075-T6 aluminium alloy joints. Mater. Des. **32**, 535–549 (2011)
10. Elangovan, K.; Balasubramanian, A.V.; Babu, S.: Predicting tensile strength of friction stir welded AA6061 aluminium alloy joints by a mathematical model. Mater. Des. **30**, 188–193 (2003)
11. Elangovan, K.; Balasubramanian, A.V.; Babu, S.: Developing an empirical relationship to predict tensile strength of friction stir welded AA2219 aluminum alloy. J. Mater. Eng. Perform. **17**, 820–830 (2008)
12. Padmanaban, G.; Balasubramanian, V.: Prediction of tensile strength and optimization of process parameters for friction stir welded AZ31B magnesium alloy. Proc. Inst. Mech. Eng. B J. Eng. Manuf. **224**, 1519–1528 (2010)
13. Safeen, W.; et al.: Predicting the tensile strength, impact toughness, and hardness of friction stir-welded AA6061-T6 using response surface methodology. Int. J. Adv. Manuf. Technol. **87**, 1765–1781 (2016)
14. Ghaffarpour, M.; Dariani, B.M.: Friction stir welding parameters optimization of heterogeneous tailored welded blank sheets of aluminium alloys 6061 and 5083 using response surface methodology. Proc. Inst. Mech. Eng. B J. Eng. Manuf. **226**, 2013–2022 (2013)
15. Ramachandran, K.K.; Murugan, N.; Kumar, S.S.: Performance analysis of dissimilar friction stir welded aluminium alloy AA5052 and HSLA steel butt joints using response surface method. Int. J. Adv. Manuf. Technol. **86**, 2373–2392 (2016)
16. ASM Metals Handbook: Fractography, vol. 12, pp. 414–439. ASM International, Ohio (1992)
17. Heinz, B.; Skrotzki, B.: Characterization of a friction-stir-welded aluminum alloy 6013. Metall. Mater. Trans. B **33**, 489–498 (2002)
18. Lohwasser, D.; Chen, Z.: Friction Stir Welding. Woodhead, New Delhi (2010)
19. Fu, R.D.; Zeng, G.U.; Sun, Z.Q.; Sun, R.C.; Li, Y.; Liu, H.J.; Liu, L.: Improvement of weld temperature distribution and mechanical properties of 7050 aluminum alloy butt joints by submerged friction stir welding. Mater. Des. **32**, 4825–4831 (2011)
20. Colegrove, P.A.; Shercliff, H.R.; Zettler, R.: Model for predicting heat generation and temperature in friction stir welding from the material properties. Sci. Technol. Weld. Join. **12**, 284–297 (2007)
21. Peel, M.J.; Steuwer, A.; Withers, P.J.; Dickerson, T.; Shi, Q.; Shercliff, H.: Dissimilar friction stir welds in AA5083–AA6082. Part I: process parameter effects on thermal history and weld properties. Metall. Mater. Trans. A **37**, 2183–2193 (2006)
22. Threadgill, P.L.; Leonard, A.J.; Shercliff, H.R.; Withers, P.J.: Friction stir welding of aluminium alloys. Int. Mater. Rev. **54**, 49–93 (2009)
23. Sato, Y.S.; Kokawa, H.: Distribution of tensile property and microstructure in friction stir weld of 6063 aluminum. Metall. Mater. Trans. **32A**, 3023–3031 (2001)
24. Farzadi, A.: Correlation between precipitate microstructure and mechanical properties in AA7075-T6 aluminum alloy friction stir welded joints. Materwiss. Werksttech. **48**(2), 151–162 (2017)
25. Schmidt, H.; Hattel, J.; Wert, J.: An analytical model for the heat generation in friction stir welding. Model. Simul. Mater. Sci. Eng **12**, 143–157 (2004)
26. Feng, A.H.; Chen, D.L.; Ma, Z.Y.: Microstructure and cyclic deformation behavior of a friction-stir-welded 7075 Al alloy. Metall. Mater. Trans. A **41**, 957–971 (2010)